Nuclear Mathematical and Computational Sciences: A Century in Review, A Century Anew
Gatlinburg, Tennessee, April 6-11, 2003, on CD-ROM, American Nuclear Society, LaGrange Park, IL (2003)

ANALYSIS OF TRANSPORT SYNTHETIC ACCELERATION FOR HIGHLY HETEROGENEOUS PROBLEMS

Jae Chang and Marvin Adams
Texas A&M University
Department of Nuclear Engineering
College Station, Texas 77843-3133
jae@tamu.edu; mladams@tamu.edu

ABSTRACT

Recent studies have shown that diffusion synthetic acceleration schemes lose effectiveness (but remain convergent) for multi-dimensional problems with strong periodic heterogeneities. We study here the behavior of transport synthetic acceleration on such problems. Our somewhat surprising result is that low-order Sn acceleration of high-order Sn iterations not only loses effectiveness on strongly heterogeneous problems, but becomes divergent. We offer both analysis and numerical results that agree on this result.

Key Words: iterative methods, synthetic acceleration, Fourier analysis, heterogeneous, Krylov methods

1. INTRODUCTION

The transport equation is an integro-differential equation with seven independent variables: spatial (3), direction (2), energy (1) and time (1). Only simple problems can be solved analytically; numerical methods must be applied to most problems of interest. Since there are large numbers of unknowns, it is impractical to directly invert the problem matrix. There is therefore considerable interest in rapidly convergent iterative methods for transport problems.

The time-independent transport equation for a non-multiplying system can be written in the following form [1]:

$$\left[\vec{\Omega}\bullet\vec{\nabla}+\sigma_t\left(\vec{r},E\right)\right]\psi\left(\vec{r},E,\vec{\Omega}\right)=\int dE'\int d\Omega'\sigma_s\left(\vec{r},E'\to E,\vec{\Omega}'\bullet\Omega\right)\psi\left(\vec{r},E',\vec{\Omega}'\right)+q_{ext}\left(\vec{r},E,\vec{\Omega}\right), \quad (1)$$

where ψ is the angular flux; σ_t is the total interaction cross section; σ_s is a differential cross section for neutrons from direction $\vec{\Omega}'$ and energy E' scattering into the interval $d\vec{\Omega}$ about $\vec{\Omega}$ and energy dE about E; and q_{ext} is the external source. We can write Eq. (1) in the following operator notation [2]:

$$L\psi = S\psi + q \quad (2)$$

where

$$L=\vec{\Omega}\bullet\vec{\nabla}+\sigma\left(\vec{r},E\right)=\text{leakage plus collision operator}, \quad (3)$$

$$S = \int dE' \int d\Omega' \sigma_s \left(\vec{r}, E' \to E, \vec{\Omega}' \bullet \Omega \right) = \text{scattering operator,} \tag{4}$$

and $q = q_{ext}$.

The simplest iteration method is source iteration, which is defined as:

$$L\psi^{(l+1)} = S\psi^{(l)} + q\,, \tag{5}$$

where $S\psi^{(0)}$ is the initial guess for the scattering source. If the initial guess is 0, then the *l*-th estimate of the angular flux is the angular flux due to particles that have scattered at most *l-1* times. If the system is optically thick and has very little absorption, source iteration converges slowly. Therefore, preconditioning or synthetic acceleration methods were developed to accelerate the convergence rate of source iteration. Synthetic acceleration is at least a two-stage iteration scheme. The first stage (high-order sweep) is a single source-iteration step, Eq. (5), except that we substitute $\psi^{(l+1/2)}$ for $\psi^{(l+1)}$:

$$L\psi^{(l+1/2)} = S\psi^{(l)} + q\,. \tag{6}$$

The goal of the second stage, low-order approximation, is to find an additive correction that when added to $\psi^{(l+1/2)}$ is a better approximation to the exact solution ψ than is $\psi^{(l+1/2)}$. If we subtract Eq. (6) from Eq. (2), we can get the exact solution from:

$$\psi = \psi^{(l+1/2)} + \left(L - S\right)^{-1} S\left(\psi^{(l+1/2)} - \psi^{(l)}\right). \tag{7}$$

However, this requires inverting the transport operator *L-S*, which is just as difficult as the original problem. Therefore, if we replace $\left(L - S\right)^{-1}$ with "low-order" approximation such that

$$M \approx \left(L - S\right)^{-1}, \tag{8}$$

where the action of *M* on a vector is easier to compute than is the action of $\left(L - S\right)^{-1}$, then we have

$$\psi^{(l+1)} = \psi^{(l+1/2)} + MS\left(\psi^{(l+1/2)} - \psi^{(l)}\right), \tag{9}$$

which combined with Eq. (6) defines the synthetic acceleration scheme.

Two well-known synthetic acceleration schemes are diffusion synthetic acceleration (DSA) and transport synthetic acceleration (TSA) [2]. The DSA scheme uses a diffusion operator as the low-order approximation. Studies have shown that DSA schemes, discretized consistently with the transport operator, are unconditionally convergent for all spatial meshes. Furthermore, these DSA schemes are highly effective (converge rapidly to the solution) for problems with uniform meshes and homogenous material properties. However, recent studies show that DSA schemes

are ineffective for some strongly heterogeneous problems. Azmy [3] has shown that, at least for certain transport discretizations, it is impossible to have a preconditioner of cell-centered diffusion-like form that is unconditionally rapidly convergent. For a problem with a Periodic Horizontal Interface (PHI), he shows with Fourier analysis and numerical results that cell-centered DSA-type preconditioners lose effectiveness as heterogeneity increases. Warsa [4] has obtained similar results for different kinds of DSA schemes and somewhat different geometric heterogeneities. The bottom line is that DSA is now known to lose effectiveness on problems with high scattering ratios and strong heterogeneities. No DSA scheme has been shown to avoid this difficulty.

Transport synthetic acceleration scheme uses a simplified transport operator as the low-order approximation. Typically, the low-order operator is easier to solve than the high-order sweep. In the "beta" TSA method [5], a fraction (β) of the scattering cross section is removed in the low-order approximation. To preserve the absorption in the low-order approximation, the total cross-section is also reduced. Furthermore, a cruder quadrature set can be used in the low-order transport problem to further reduce its computational cost.

Given the recently discovered "flaw" in DSA, we would like to know whether TSA methods also suffer the same type of degradation in strongly heterogeneous problems. Our initial conjecture was that they would not be as affected as are DSA schemes because their low-order operators more closely resemble the high-order operator. As we show in this paper, we were mistaken. TSA schemes that are rapidly convergent for homogeneous problems are *divergent* for problems with moderately high scattering ratios and moderately strong heterogeneities.

In this paper we analyze the performance of the simplest TSA schemes – ones in which only the low-order quadrature sets (not any cross sections) differ from the high-order operator. This is the β=0 scheme, which is just low-order S_n acceleration of high-order S_n iteration. In the next section, we will present the TSA scheme. In section 3, we will present results from a Fourier analysis of the β=0 TSA scheme for PHI-like problems using diamond differencing for spatial discretization. In section 4, we show some numerical results, which agree with our Fourier analysis. In the final section we present some observations and conclusions.

2. TRANSPORT SYNTHETIC ACCELERATION

In this section we describe the "beta" transport synthetic acceleration scheme. Complete presentations of beta TSA can be found in reference [5]. For the discrete-ordinates transport equation with isotropic scattering and for a single energy group, beta TSA iteration is defined by the following equations:

$$\vec{\Omega}_m \bullet \vec{\nabla} \psi_m^{(l+1/2)}(\vec{r}) + \sigma_t(\vec{r}) \psi_m^{(l+1/2)}(\vec{r}) = \frac{\sigma_s(\vec{r})}{4\pi} \phi^{(l+1/2)}(\vec{r}) + \frac{q(\vec{r})}{4\pi} , \tag{10}$$

$$\phi^{(l+1/2)}(\vec{r}) = \sum_{m=1}^{M} w_m \psi_m^{(l+1/2)}(\vec{r}) , \tag{11}$$

$$\vec{\Omega}_n \bullet \vec{\nabla} f_n^{(k+1/2)}(\vec{r}) + \left[\sigma_t(\vec{r}) - \beta\sigma_s(\vec{r})\right] f_n^{(k+1/2)}(\vec{r}) = \frac{\sigma_s(\vec{r})(1-\beta)}{4\pi} F^{(k+1/2)}(\vec{r}) + \frac{\sigma_s(\vec{r})}{4\pi}\left[\phi^{(l+1/2)}(\vec{r}) - \phi^{(l)}(\vec{r})\right], \tag{12}$$

$$F^{(k+1/2)}(\vec{r}) = \sum_{n=1}^{N} w_n f_n^{(k+1/2)}(\vec{r}), \tag{13}$$

$$\phi^{(l+1)}(\vec{r}) = \phi^{(l+1/2)}(\vec{r}) + F^{(k+1/2)}(\vec{r}). \tag{14}$$

This iteration scheme is efficient only if the number of high order iterations is reduced without a large penalty for solving the low-order calculations. There are adjustable parameters in this method. The amount of scattering removed in the low-order problem is controlled by beta (β). The number of quadrature directions in the low-order problem (N) can be smaller than the number in the high-order problem (M), and therefore should require less computation. Furthermore, the number of low-order iterations (k) can be set to a fixed value instead of fully converging the low-order problem. It should be noted that if the high-order and low-order quadrature are equal (M=N) and β=0, the problem will converge immediately, because the low-order problem is identical to the high-order problem.

Unlike DSA, which requires consistent discretization of the diffusion operator with respect to the transport operator, TSA does not require any special effort or coding to consistently discretize the low-order operator, because both high- and low-order operators use the same spatial discretization. In a computer code for discrete-ordinates transport we can implement TSA by re-using the transport-sweep coding that already exists in the code.

3. FOURIER ANALYSIS

In this section we present a two-dimensional Fourier analysis of a PHI problem (see Figure 1) for TSA with the Diamond Difference (DD) spatial discretization. Fourier analysis is used to analyze the error modes of iteration schemes. If we consider equations for iteration errors instead of fluxes, they are identical to Eqs. (10) – (14) except that $q(\vec{r}) = 0$.

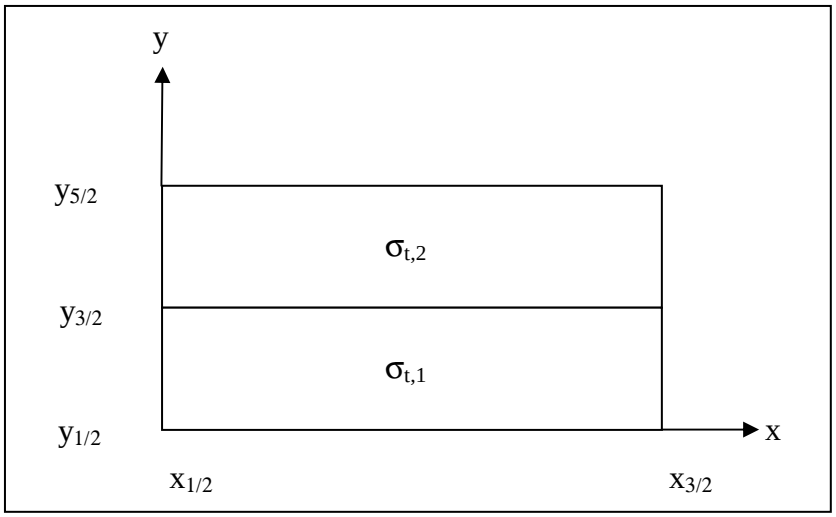

Figure 1. PHI problem.

The PHI problem consists of a two-cell block with total cross sections $\sigma_{t,1}$ and $\sigma_{t,2}$. We assumed the two-cell block repeats periodically. The separation-of-variable ansatz for a given mode is:

$$\psi_{m,j}^{\left(l+\frac{1}{2}\right)} = \omega^{(l)} a_{m,j} e^{i\left(\lambda_x x_1 + \lambda_y y_j\right)}, \tag{15}$$

$$\psi_{m,1\pm\frac{1}{2},j}^{\left(l+\frac{1}{2}\right)} = \omega^{(l)} b_{m,1\pm\frac{1}{2},j} e^{i\left(\lambda_x x_{1\pm\frac{1}{2}} + \lambda_y y_j\right)}, \tag{16}$$

$$\psi_{m,j+\frac{1}{2}}^{\left(l+\frac{1}{2}\right)} = \omega^{(l)} d_{m,j} e^{i\left(\lambda_x x_1 + \lambda_y y_{j+\frac{1}{2}}\right)}, \tag{17}$$

$$\psi_{m,\frac{1}{2}}^{\left(l+\frac{1}{2}\right)} = \omega^{(l)} d_{m,2} e^{i\left(\lambda_x x_1 + \lambda_y y_{\frac{1}{2}}\right)} \tag{18}$$

$$\phi_j^{\left(l+\frac{1}{2}\right)} = \omega^{(l)} A_j e^{i\left(\lambda_x x_1 + \lambda_y y_j\right)}, \tag{19}$$

$$\phi_j^{(l)} = \omega^{(l)} B_j e^{i\left(\lambda_x x_1 + \lambda_y y_j\right)}, \tag{20}$$

$$f_{n,j} = \omega^{(l)} \tilde{a}_{n,j} e^{i\left(\lambda_x x_1 + \lambda_y y_j\right)}, \tag{21}$$

$$f_{n,1\pm\frac{1}{2},j} = \omega^{(l)} \tilde{b}_{n,1\pm\frac{1}{2},j} e^{i\left(\lambda_x x_{1\pm\frac{1}{2}} + \lambda_y y_j\right)}, \tag{22}$$

$$f_{n,j+\frac{1}{2}} = \omega^{(l)} \tilde{d}_{n,j} e^{i\left(\lambda_x x_1 + \lambda_y y_{j+\frac{1}{2}}\right)}, \tag{23}$$

$$f_{n,\frac{1}{2}} = \omega^{(l)} \tilde{d}_{n,2} e^{i\left(\lambda_x x_1 + \lambda_y y_{\frac{1}{2}}\right)} \tag{24}$$

$$F_j = \omega^{(l)} \tilde{A}_j e^{i\left(\lambda_x x_1 + \lambda_y y_j\right)}, \tag{25}$$

$$\phi_j^{\left(l+\frac{1}{2}\right)} - \phi_j^{(l)} = \omega^{(l)} \tilde{B}_j e^{i\left(\lambda_x x_1 + \lambda_y y_j\right)}, \tag{26}$$

where *j=1,2*.

After substituting the ansatz into the DD error equations and performing some algebra, we obtain:

$$\omega \vec{b} = X \vec{b}, \tag{27}$$

where *X* is a 2 x 2 iteration matrix and ω are the eigenvalues.

The iteration eigenvalues are functions of the problem parameters: material properties $\sigma_{t,1}$, $\sigma_{t,2}$ and the scattering ratio, dimensions Δx and Δy, and parameters $\left[\theta_x, \theta_y\right] \in [0,\pi] \times [0,\pi]$, where $\theta_{x_i} = \lambda_x \Delta x_i, \theta_{y_j} = \lambda_y \Delta y_j$ and λ_x and λ_y are Fourier wave numbers. A Fortran code was used to search through the parameters to find the maximum eigenvalue in magnitude, which is the spectral radius for the iteration scheme for the problem analyzed.

For our analysis, we set the cell widths to $\Delta x = \Delta y = 1$, varied the total cross sections from 10^{-4} to 10^{4}, and varied the scattering ratios *c* = 0.9, 0.99, 0.999, and 0.9999. Tables I – IV are the results for S4/S2, which means an S4 high-order quadrature and the S2 low-order TSA scheme with β=0.

Table I. S4/S2 spectral radii for c=0.9

$\sigma_{t,2}$	$\sigma_{t,1}$								
	1.00E-04	**1.00E-03**	**1.00E-02**	**1.00E-01**	**1.00E+00**	**1.00E+01**	**1.00E+02**	**1.00E+03**	**1.00E+04**
1.00E-04	0.5455	3.0000	5.4544	5.9243	4.8198	1.3633	1.4945	1.4601	0.9773
1.00E-03	3.0000	0.5455	2.9999	5.4394	4.7748	1.3589	1.4699	1.4863	1.4428
1.00E-02	5.4544	2.9999	0.5455	2.9902	4.3690	1.3166	1.3855	1.4587	1.4098
1.00E-01	5.9243	5.4394	2.9902	0.5455	2.3259	1.0130	1.1640	1.3752	1.4586
1.00E+00	4.8198	4.7748	4.3690	2.3259	0.5455	0.5455	0.7494	1.1564	1.3751
1.00E+01	1.3633	1.3589	1.3166	1.0130	0.5455	0.5455	0.5455	0.7462	1.1563
1.00E+02	1.4945	1.4699	1.3855	1.1640	0.7494	0.5455	0.5455	0.5455	0.5455
1.00E+03	1.4601	1.4863	1.4587	1.3752	1.1564	0.7462	0.5455	0.5455	0.5455
1.00E+04	0.9773	1.4428	1.4098	1.4586	1.3751	1.1563	0.5455	0.5455	0.5455

Table II. S4/S2 spectral radii for c=0.99

$\sigma_{t,2}$ \ $\sigma_{t,1}$	1.00E-04	1.00E-03	1.00E-02	1.00E-01	1.00E+00	1.00E+01	1.00E+02	1.00E+03	1.00E+04
1.00E-04	0.6535	6.0000	32.9991	59.8358	52.5455	8.4053	16.2491	16.0582	10.6961
1.00E-03	6.0000	0.6535	5.9998	32.9081	48.2251	8.3380	15.8562	15.9890	6.0773
1.00E-02	32.9991	5.9998	0.6535	5.9805	26.4077	7.7177	13.3697	15.0222	14.8117
1.00E-01	59.8358	32.9081	5.9805	0.6535	4.6894	4.3402	7.8391	12.3918	15.0233
1.00E+00	52.5455	48.2251	26.4077	4.6894	0.6535	0.6931	2.5525	7.4114	12.3835
1.00E+01	8.4053	8.3380	7.7177	4.3402	0.6931	0.6535	0.6535	2.4906	7.4072
1.00E+02	16.2491	15.8562	13.3697	7.8391	2.5525	0.6535	0.6535	0.6535	2.4903
1.00E+03	16.0582	15.9890	15.0222	12.3918	7.4114	2.4906	0.6535	0.6535	0.6535
1.00E+04	10.6961	6.0773	14.8117	15.0233	12.3835	7.4072	2.4903	0.6535	0.6535

Table III. S4/S2 spectral radii for c=0.999

$\sigma_{t,2}$ \ $\sigma_{t,1}$	1.00E-04	1.00E-03	1.00E-02	1.00E-01	1.00E+00	1.00E+01	1.00E+02	1.00E+03	1.00E+04
1.00E-04	0.6653	6.5941	60.5438	332.0888	486.8490	45.5143	147.1761	161.7595	107.8742
1.00E-03	6.5941	0.6653	6.5938	60.3768	267.6492	41.7949	142.2910	152.6177	61.3201
1.00E-02	60.5438	6.5938	0.6653	6.5727	48.4520	23.1795	107.0523	125.6114	146.6165
1.00E-01	332.0888	60.3768	6.5727	0.6653	5.1620	6.5176	31.3509	75.4839	125.7545
1.00E+00	486.8490	267.6492	48.4520	5.1620	0.6653	0.7564	4.0897	24.3520	75.5200
1.00E+01	45.5143	41.7949	23.1795	6.5176	0.7564	0.6653	0.6653	3.8807	24.3590
1.00E+02	147.1761	142.2910	107.0523	31.3509	4.0897	0.6653	0.6653	0.6653	3.8787
1.00E+03	161.7595	152.6177	125.6114	75.4839	24.3520	3.8807	0.6653	0.6653	0.6653
1.00E+04	107.8742	61.3201	146.6165	125.7545	75.5200	24.3590	3.8787	0.6653	0.6653

Table IV. S4/S2 spectral radii for c=0.9999

$\sigma_{t,2}$	$\sigma_{t,1}$								
	1.00E-04	**1.00E-03**	**1.00E-02**	**1.00E-01**	**1.00E+00**	**1.00E+01**	**1.00E+02**	**1.00E+03**	**1.00E+04**
1.00E-04	0.6665	6.6593	65.9982	604.3418	2680.0818	412.9556	728.4131	1601.0800	1079.3987
1.00E-03	6.6593	0.6665	6.6591	65.8162	487.0734	227.4966	677.9043	1346.4121	613.2035
1.00E-02	65.9982	6.6591	0.6665	6.6378	52.8174	42.0237	388.9780	784.9370	1248.0668
1.00E-01	604.3418	65.8162	6.6378	0.6665	5.2140	6.8847	56.1533	245.2290	739.9359
1.00E+00	2680.0818	487.0734	52.8174	5.2140	0.6665	0.7640	4.4589	38.7260	245.9246
1.00E+01	412.9556	227.4966	42.0237	6.8847	0.7640	0.6665	0.6665	4.1981	38.7570
1.00E+02	728.4131	677.9043	388.9780	56.1533	4.4589	0.6665	0.6665	0.6665	4.1956
1.00E+03	1601.0800	1346.4121	784.9370	245.2290	38.7260	4.1981	0.6665	0.6665	0.6665
1.00E+04	1079.3987	613.2035	1248.0668	739.9359	245.9246	38.7570	4.1956	0.6665	0.6665

We were somewhat surprised by the results of the Fourier analysis. We had conjectured that because we were using a transport operator in the low-order problem, we would not experience the degradations seen in DSA schemes. Not only do we observe degradation with heterogeneity, but also the iteration scheme diverges for many cases. For all divergent cases, the large-magnitude eigenvalues were real and negative. Spectral radii increase when the scattering ratios increase. For all homogeneous cases, $\sigma_{t,1} = \sigma_{t,2}$, the spectral radii behave as expected: they are bounded below *c*, they increase as a function of the scattering ratio, and for a given scattering ratio they are independent of total cross sections.

Results from the Fourier analysis for S6/S2 and S6/S4 iteration schemes are presented in Tables V and VI, respectively. The scattering ratios for both cases are 0.9. The results from the S6/S2 iteration exhibit characteristics similar to those of the S4/S2 iteration with regards to different cross sections. For problems with large heterogeneities, the spectral radius for S6/S2 iteration scheme is smaller than that of S4/S2. As the differences in heterogeneity become smaller, spectral radii for S6/S2 become larger than those of the S4/S2 scheme.

Results for S12/S2 and S12/S4 iteration schemes for c=0.9 are listed in Tables VII and VIII, respectively. The results have the same characteristics as the previous cases. Using the S4 quadrature in the low-order calculations reduces the spectral radius compared to using an S2 low-order quadrature. However, this requires more computations in the low-order calculations. When the scattering ratio is increased, the spectral radius also increases as it does with the S4/S2 scheme, and we find that using S4 for the low-order quadrature set is not always convergent. Table IX is a list of the spectral radius for $\sigma_{t,1}$=1 and $\sigma_{t,2}$=10^4 for various scattering ratio for both S6/S4 and S12/S4 iteration schemes.

Table V. S6/S2 spectral radii for c=0.9

$\sigma_{t,2}$	$\sigma_{t,1}$				
	1.00E-04	**1.00E-02**	**1.00E+00**	**1.00E+02**	**1.00E+04**
1.00E-04	0.5455	5.4544	4.7918	1.1419	0.7653
1.00E-02	5.4544	0.5455	4.3409	0.8438	0.7866
1.00E+00	4.7918	4.3409	0.5455	0.5455	0.7356
1.00E+02	1.1419	0.8438	0.5455	0.5455	0.5455
1.00E+04	0.7653	0.7866	0.7356	0.5455	0.5455

Table VI. S6/S4 spectral radii for c=0.9

$\sigma_{t,2}$	$\sigma_{t,1}$				
	1.00E-04	**1.00E-02**	**1.00E+00**	**1.00E+02**	**1.00E+04**
1.00E-04	0.1764	0.4166	0.1938	0.7792	0.7653
1.00E-02	0.4166	0.1763	0.1896	0.6939	0.7813
1.00E+00	0.1938	0.1896	0.1761	0.2502	0.6888
1.00E+02	0.7792	0.6939	0.2502	0.1763	0.2503
1.00E+04	0.7653	0.7813	0.6888	0.2503	0.1763

Table VII. S12/S2 spectral radii for c=0.9

$\sigma_{t,2}$	$\sigma_{t,1}$				
	1.00E-04	**1.00E-02**	**1.00E+00**	**1.00E+02**	**1.00E+04**
1.00E-04	0.6980	6.9794	5.2503	0.9726	0.7157
1.00E-02	6.9794	0.6980	4.7487	0.7222	0.7156
1.00E+00	5.2503	4.7487	0.6980	0.6980	0.7113
1.00E+02	0.9726	0.7222	0.6980	0.6980	0.6980
1.00E+04	0.7157	0.7156	0.7113	0.6980	0.6980

Table VIII. S12/S4 spectral radii for c=0.9

$\sigma_{t,2}$	$\sigma_{t,1}$				
	1.00E-04	**1.00E-02**	**1.00E+00**	**1.00E+02**	**1.00E+04**
1.00E-04	0.1765	0.4204	0.3233	0.5966	0.5997
1.00E-02	0.4204	0.1764	0.3167	0.5707	0.5972
1.00E+00	0.3233	0.3167	0.1764	0.3487	0.5710
1.00E+02	0.5966	0.5707	0.3487	0.1764	0.3488
1.00E+04	0.5997	0.5972	0.5710	0.3488	0.1765

Table IX. Spectral radius for S6/S2, S6/S4, S12/S2,S12/S2 for $\sigma_{t,1}$=1 and $\sigma_{t,2}$=10^4

c	S6/S2	S6/S4	S12/S2	S12/S4
0.9	0.7356	0.6888	0.7113	0.5710
0.99	6.8206	6.0073	3.0132	2.9136
0.999	43.6095	31.8169	19.1057	18.0083
0.9999	157.6343	78.8965	73.3839	64.3731

4. NUMERICAL RESULTS

In this section, we present numerical calculations performed to test the predictions of the Fourier analysis. The calculations were done using a parallel transport code written at Texas A&M University. The dimensions of the test problem are 100 cm x 200 cm x 10^6 cm. There are 100 cells in the x direction (Δx = 1 cm), 200 cells in the y direction (Δy = 1 cm), and 3 cells in the z direction ($\Delta z_1 = 1\text{cm},\ \Delta z_2 = 999999$ cm, $\Delta z_3 = 1$ cm). The problem is separated into columns in the z directions. The first column (x = 0-100 cm, y = 0-200 cm, z = 0-1 cm) and the third column (x = 0-100 cm, y = 0-200 cm, z = 999999–10^6 cm) have homogenous material properties (total cross section = $\sigma_{t,1}$). The second column consists of 200 xz-planes of cells with alternating materials in the y direction; see Figure 2. There are isotropic incident boundary sources on the left and bottom face of the problem and vacuum on other four remaining boundary faces.

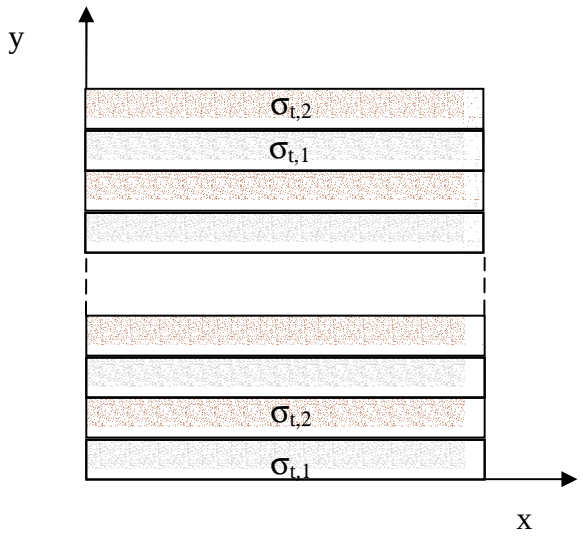

Figure 2. Test problem.

The convergence tolerance for both high and low-order was set to 10^{-7}. However, the maximum number of low-order sweeps was set to 500 iterations. For all cases, β was set to zero. The spectral radius for the numerical problem was estimated by taking the ratio of L_2-norms of residuals of successive iterations:

$$\rho \approx \frac{\left\| \phi^{(l+1)} - \phi^{(l)} \right\|_2}{\left\| \phi^{(l)} - \phi^{(l-1)} \right\|_2}. \tag{28}$$

For the first problem, the high-order quadrature was S4 quadrature and the low-order problem used the S2 quadrature. Both cross sections, $\sigma_{t,1}$ and $\sigma_{t,2}$, were varied, and the scattering ratio was 0.9. Table X contains both the numerical results and the Fourier analysis results (from the previous section) for c = 0.9.

Table X. S4/S2 spectral radius for c=0.9

$\sigma_{t,2}$	$\sigma_{t,1}$=1.0E-04		$\sigma_{t,1}$=1.0		$\sigma_{t,1}$=1.0E4	
	numerical	Fourier	numerical	Fourier	numerical	Fourier
1.00E-04	0.0014	0.5455	4.5255	4.8213	0.0397	1.4987
1.00E-02	0.0793	5.4544	4.1231	4.3690	0.1745	1.4867
1.00E+00	4.5254	4.8213	0.4639	0.5455	0.4521	1.3751
1.00E+02	1.1009	1.4945	0.4741	0.7494	0.0783	0.7461
1.00E+04	0.0398	1.4987	0.4562	1.3751	0.0089	0.5455

The numerical estimates agree with the Fourier analysis for many of these problems; where there is disagreement we believe we understand why. The spectral radii for thin problems (small cross sections) are smaller than the Fourier analysis predicts because of leakage in the problems, which speeds convergence. (The Fourier analysis assumes an infinite medium.) The spectral radii for thick problems (large cross sections) are smaller because there are only a few divergent modes, which are very difficult to excite in the numerical test problems. The problems often converge before those modes have a chance to become dominant. We discuss this in more detail below.

As a further test of the analysis we examine the spatial shape of a divergent error mode in a computational problem and compare against analysis predictions. For $\sigma_{t,1}$=1.0 and $\sigma_{t,2}$ = 10^{-4}, the Fourier analysis predicts that the spectral radius occurs near $\left[\theta_x = \frac{\pi}{2}, \theta_y = \frac{\pi}{2}\right]$ mode. This indicates cell-by-cell oscillations with the following pattern in the scalar flux: positive, zero, negative, zero, positive, etc., in both directions. Figure 3 is a XY slice of the computed numerical solution in this problem after many iterations. The mesh lines in Figure 3 cross at the cell centers. The figure shows the scalar flux oscillating as predicted by the Fourier analysis. Thus, not only is the observed rate of divergence in agreement with the analysis, but also the numerically observed divergent error mode is exactly as predicted.

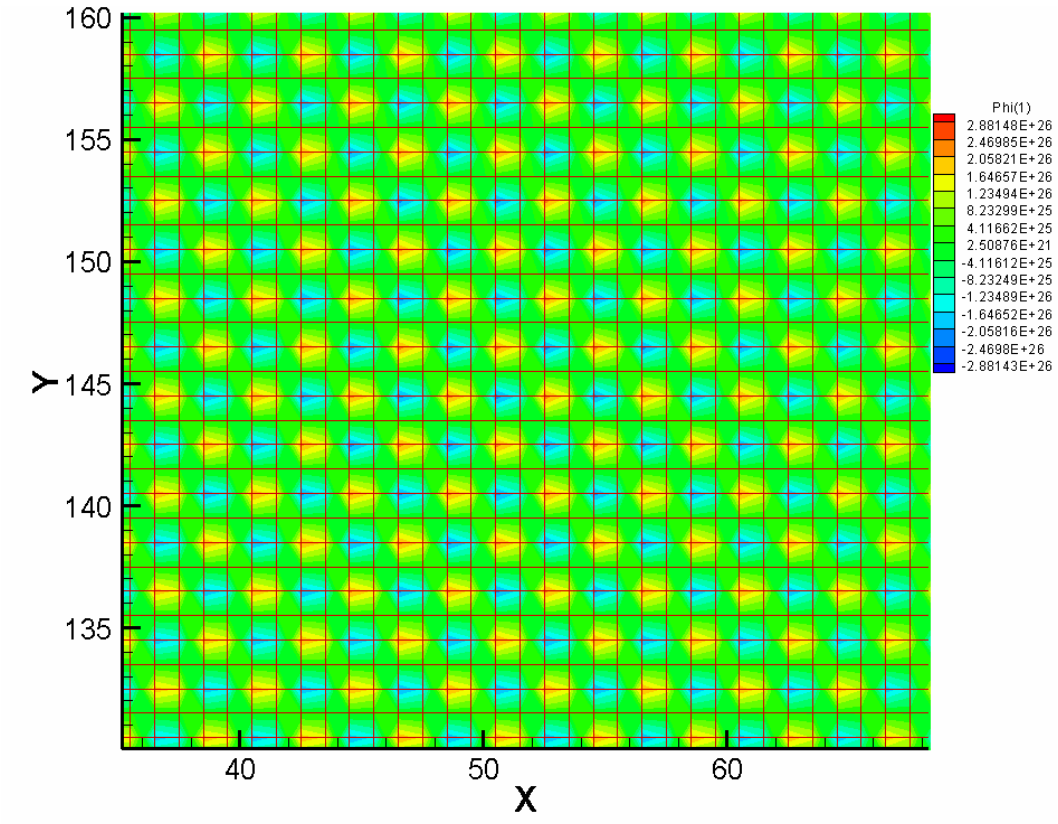

Figure 3. XY slice of the numerical problem

As noted above, for some optically thick problems the numerically estimated spectral radii were much smaller than the results from the Fourier analysis. Figure 4 is a plot of iteration eigenvalues as function of θ_x and θ_y for c=0.9, $\sigma_{t,1}$ = 1.0 and $\sigma_{t,2}$ = 10^4, as calculated by the Fourier analysis. From this figure, it would appear that the spectral radius is approximately 0.6 instead of the value of 1.37 reported in the table above. However, if we "zoom in" near $(\theta_x = \pi, \theta_y = \pi)$, we find a line of very narrow peaks where the eigenvalues have magnitude greater than 1. See Figure 5 and note the expanded scale. Because only a very small set of error modes have large eigenvalue-magnitudes, we believe that the numerical problem does not excite those modes and thus does not observe divergence (or even slow convergence).

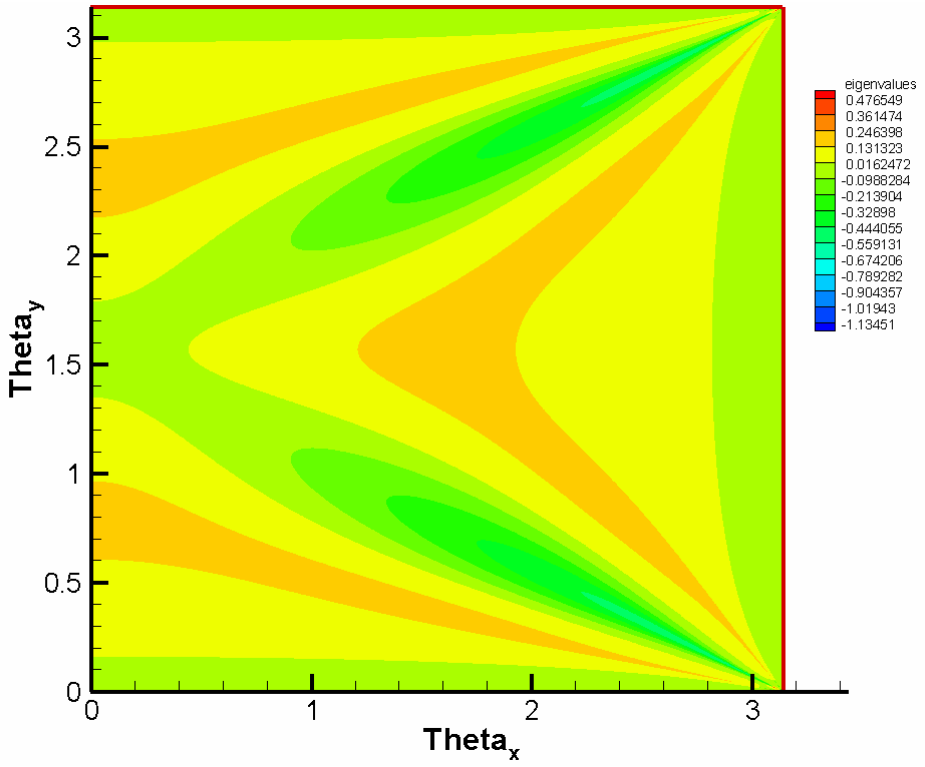

Figure 4. Iteration error eigenvalues for c=0.9 and $\sigma_{t,1}$ = 1.0 and $\sigma_{t,2}$ = 10^4.

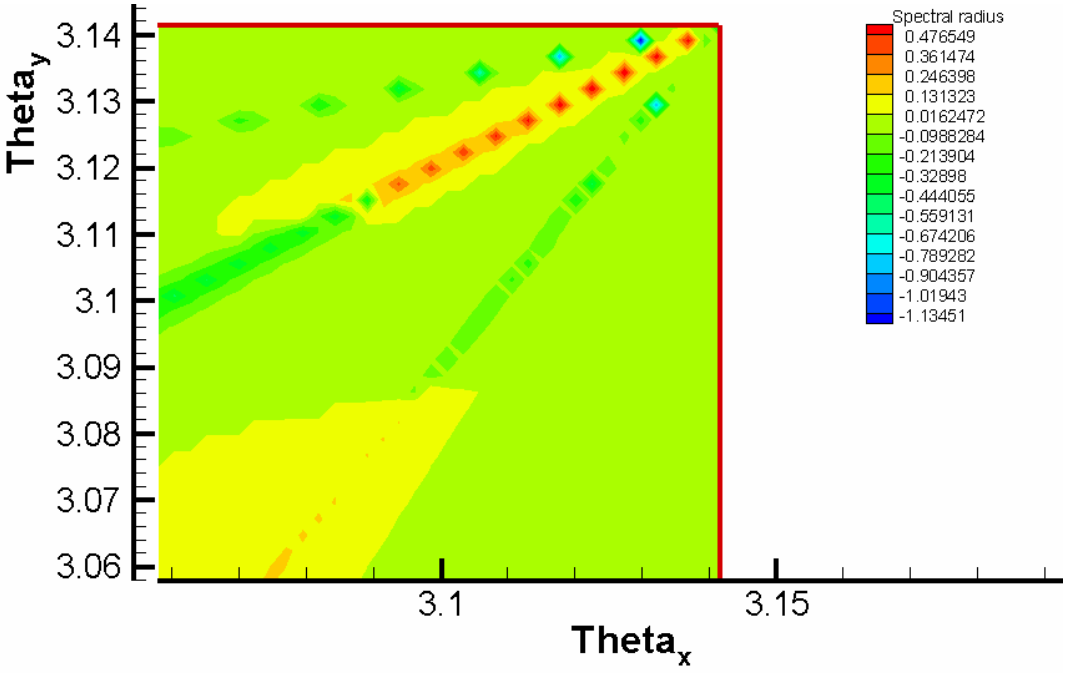

Figure 5. Iteration error eigenvalues for c=0.9 and $\sigma_{t,1}$ = 1.0 and $\sigma_{t,2}$ = 10^4. Note the tiny islands of blue.

Tables XI and XII are the numerical and Fourier analysis results for the S6/S2 and S6/S4 schemes. The numerical results are smaller than the Fourier analysis due to some leakage in the numerical problem. As in the case for S4/S2 scheme, for optically thick problem ($\sigma_{t,2}$ =10^4) the numerical spectral radius is smaller than the one calculated from Fourier analysis.

Table XI. S6/S2 spectral radius for $\sigma_{t,1}$=1.0

$\sigma_{t,2}$	c=0.9		c=0.99	
	numerical	Fourier	numerical	Fourier
1.00E-04	4.5046	4.7918	32.5264	52.2256
1.00E-02	4.1027	4.3409	20.1193	26.2765
1.00E+00	0.4591	0.5455	0.5865	0.6535
1.00E+02	0.4632	0.5455	1.2958	1.6978
1.00E+04	0.4508	0.7356	0.5458	6.8206

Table XII. S6/S4 spectral radius for $\sigma_{t,1}$=1.0

$\sigma_{t,2}$	c=0.9		c=0.99	
	numerical	Fourier	numerical	Fourier
1.00E-04	0.1722	0.1938	0.1889	0.2294
1.00E-02	0.1564	0.1896	0.1834	0.2243
1.00E+00	0.0599	0.1761	0.0516	0.1972
1.00E+02	0.1476	0.2502	0.4674	0.7066
1.00E+04	0.0220	0.6888	0.0264	6.0073

From the numerical results presented here, and many more not shown, we conclude that our Fourier analysis is correct and that low-order SN acceleration of high-order SN iterations can indeed diverge for multi-dimensional problems with strong heterogeneities.

5. CONCLUSIONS

We have examined the performance of the transport synthetic acceleration iteration scheme with β=0 for problems with heterogeneity between cells. This iteration scheme is equivalent to low-order Sn acceleration of Sn iterations. Fourier analysis of S4/S2, S6/S2, S6/S4, S12/S2, and S12/S4 were conducted for a variety of heterogeneous problems with periodic horizontal interfaces. The Fourier analysis revealed that for many cases this TSA scheme is divergent, with some real and negative eigenvalues having magnitudes greater than unity. Spectral radii decreased when the low-order quadrature was increased from S2 to S4. Numerical calculations were performed on a parallel transport code and the calculated spectral radii were compared to the results from the Fourier analysis. Leakage in the optically thin problems caused smaller spectral radii in the numerical calculations. For some optically thick problems, the Fourier analysis reveals that the divergent eigenvalues are associated with extremely small regions of Fourier-parameter space. Thus, it is not surprising that the numerical calculations did not excite these error modes. For other problems the numerical calculations agreed with the analysis, diverging exactly as predicted.

Although it is discouraging to find spectral radii greater than one, the eigenvalues whose magnitudes exceed unity are always real and negative. This provides a potential opportunity to perform simple operations that damp the previously divergent iteration errors, thus salvaging the scheme. Here "simple operations" include taking linear combinations of recent iterates or imbedding the TSA iteration inside a Krylov solver such as Conjugate Gradient or GMRES. With such methods it can be shown that the error for (l+1)th iteration, $\phi^{(l+1)}$, is a linear combination of previous iterates, with the combination chosen to minimize the (l+1)th residual in a certain norm [2].

It is well known that Krylov methods can converge problems for which preconditioned Richardson iteration alone diverges. (Synthetic acceleration methods are preconditioned Richardson iterations [2].) We offer here a simple illustration of how a linear combination of iterates (and thus errors) can converge rapidly even when the underlying iteration scheme diverges with a large negative eigenvalue. Let us define the error for the *l*-th iteration as $\phi^{(l)}$ and the error after one synthetic iteration as $\phi^{(l+2/3)} = \omega\phi^{(l)}$, where ω is the eigenvalue of the synthetic iteration scheme. Consider now the following new iteration scheme, in which the error for the next iteration $\phi^{(l+1)}$ is a linear combination of the errors at the *l*-th iteration and after one synthetic iteration:

$$\begin{aligned}\phi^{(l+1)} &= \alpha\phi^{(l+2/3)} + (1-\alpha)\phi^{(l)} \\ &= \alpha\omega\phi^{(l)} + (1-\alpha)\phi^{(l)} \\ &= \left[\alpha\omega + (1-\alpha)\right]\phi^{(l)}.\end{aligned} \tag{29}$$

The eigenvalue of the synthetic iteration is ω, the eigenvalue of the proposed scheme is [$\alpha\omega$ + 1-α], and α is an adjustable parameter. If the values of ω are known for all error modes, and only negative values have magnitudes greater than unity, then there is a value of α that causes the proposed scheme's spectral radius to be less than unity. For example, suppose that ω is known to range from -5.0 to +0.5. Then the choice α = 4/13 produces new eigenvalues that range from -11/13 to + 11/13; thus the new scheme would converge reasonably quickly.

We hope to explore using Krylov methods to develop a convergent iteration scheme based on TSA further in the near future. We have also found that loose convergence of the low-order problem can improve TSA performance relative to complete convergence of the low-order problem. This also begs for further study.

This paper is limited only to β=0. We expect to conduct further studies varying β and number of low-order iterations. Finally, there exist versions of TSA that are alternatives to the "beta" method discussed here. One such alternative reduces the scattering cross section in such a way that the diffusion length remains unchanged (whereas the beta method reduces the scattering cross section but holds the absorption cross section constant). We hope to explore in the near future all of these variants for heterogeneous problems.

REFERENCES

1. J. J. Duderstadt and W. R. Martin, *Transport Theory*, Wiley-Interscience, New York (1979).
2. M. L. Adams and E. W. Larsen, "Fast Iterative Methods for Discrete-Ordinates Particle Transport Calculations," *Prog. Nucl. Energy*, **40**, 3 (2002).
3. Y. Y. Azmy, "Unconditionally Stable and Robust Adjacent-Cell Diffusive Preconditioning of Weighted-Difference Particle Transport Methods is Impossible," *Journal of Computational Physics*, **182**, 213 (2002).
4. J. Warsa, Personal communication (2002).
5. G. L. Ramone, M. L. Adams, and P. F. Nowak, "A Transport Synthetic Acceleration Method for Transport Iterations," *Nucl. Sci. Eng.*, **125**, 257 (1997).